

**EOS IDS Volcanology Team
Data Product Document
Product # 3296**

Volcano Temperature Change

Version 3

November 6, 1995

**Vincent J. Realmuto
Jet Propulsion Laboratory
vince@vulcano.jpl.nasa.gov**

Table Of Contents

| | |
|---|----|
| 1. Introduction | 1 |
| 1.1 Algorithm and Product Description | 1 |
| 1.2 Document Scope | 1 |
| 1.3 Relevant Documents | 1 |
| 2. Overview and Background Information | 1 |
| 2.1 Experiment Objective | 1 |
| 2.2 Historical Perspective | 1 |
| 2.3 Instrument Characteristics | 2 |
| 3. Algorithm Description | 2 |
| 3.1 Theoretical Description | 2 |
| 3.2 Practical Considerations | 3 |
| 3.2.1 Operation of Procedure | 3 |
| 3.2.2 Input Data Requirements | 4 |
| 3.2.3 Output Data Products | 4 |
| 4. Constraints, Limitations, and Assumptions | 5 |
| 5. References | 6 |
| 6. Appendices | 8 |
| Appendix A: Examples of Output from XCHANGE2 | 8 |
| Appendix B: XCHANGE2 On-line Help Documentation | 12 |

List of Tables

| | |
|--|---|
| Table 1: Characteristics of the ASTER Channels | 7 |
|--|---|

1. INTRODUCTION

1.1 Algorithm and Product Identification

This document describes an algorithm for the detection of significant changes in the surface temperature of volcanic features using data acquired by the Advanced Spaceborne Thermal Emission and Reflectance Radiometer (ASTER). ASTER is currently scheduled for a 1998 launch on the AM-1 Earth Observing System (EOS) platform. This data product is number 3296, Volcano Temperature Change, of the Global Assessment of Active Volcanism Interdisciplinary Science (IDS) Team. This team is led by Dr. Peter J. Mouginis-Mark of the University of Hawaii at Manoa.

1.2 Document Scope

This document contains a brief description of Student's t test, a statistical procedure for analysis and data testing. Detailed discussions of this test or the theoretical framework of probability and statistics are beyond the scope of this document. Davis [1973] or Frieden [1983] contain thorough discussions of these topics.

The following sections contain an overview of the remote sensing of surface temperatures at volcanoes, a discussion of the operation of a procedure designed to map temporal changes in surface temperature, and an example resulting from the application of the change-detection procedure to image data acquired over Mount St. Helens Volcano, Washington. The background material and operating instructions provided by this document will enable investigators to apply the change-detection procedure to their volcanic field sites.

1.3 Relevant EOS Documents

Gillespie et al., Temperature Emissivity Separation Algorithm Theoretical Basis Document (ATBD-AST-03)

Guenther et al., MODIS Level 1B Algorithm Theoretical Basis Document (ATBD-MOD-01)

Menzel WP and Gumley LE, MODIS Atmospheric Profile Retrieval Algorithm Theoretical Basis Document (ATBD-MOD-07)

Palluconi et al, Atmospheric Correction Methods for ASTER Radiometry (ATBD-AST-04)

Watanabe et al., Algorithm Theoretical Basis Document for ASTER Level 1 Data Processing (ATBD-AST-01)

2. OVERVIEW AND BACKGROUND INFORMATION

2.1 Experiment Objective

The objective of the experiment described in this document is to use satellite-based sensors to map temporal changes in the surface temperature of several select volcanoes. The ability to map such changes from space will be a valuable asset to volcano monitoring programs, since such measurements are often impractical or even dangerous to obtain. Satellite-based remote sensing is the only mapping technique that can produce a virtually instantaneous image, or map, of surface temperature distributions over large (3600 km² per scene, in the case of ASTER) areas. In addition, the repetitive coverage provided by satellite-based sensors will facilitate the separation of temporal temperature changes due to volcanic or geothermal activity from those due to normal diurnal and seasonal variations in insolation and local weather conditions. A chronology of temperature maps is required to characterize the diurnal and seasonal variations in surface temperature.

2.2 Historical Perspective

The direct measurement of the surface temperature of volcanic features is not practical or safe in many field settings. Thermal infrared (TIR) remote sensing of surface temperatures offers an al-

ternative to direct measurements, and this mapping technique has been applied to a variety of volcanoes since the early 1960's.

Airborne remote sensing surveys of volcanic and geothermal regions have been conducted in Hawaii [Fischer et al., 1964; Realmuto et al., 1992], Iceland [Friedman and Williams, 1970; Palmason et al., 1970], various Cascade Volcanoes [Moxham, 1970; Friedman and Frank, 1980; Friedman et al., 1981 and 1982; Kieffer et al., 1981], Italy [Friedman and Williams, 1968; Bianchi et al., 1990, Abrams et al., 1994], Costa Rica, Antarctica, and the Philippines [Friedman and Williams, 1968].

Current satellite-based TIR sensors provide repetitive coverage but at very coarse spatial resolution. TIR image data collected with the Landsat Thematic Mapper (TM) and Advanced Very High Resolution Radiometer (AVHRR) have spatial resolutions (at nadir) of 120 m and 1 km, respectively. Recent examples of the use of TM and AVHRR thermal imagery to map volcanic features can be found in Bonneville and Gouze [1992], Flynn et al. [1994], Gaonac'h et al. [1994], and Mouginis-Mark et al. [1994].

Single-channel thermal imaging systems were employed in the majority of the aforementioned investigations. Since TIR radiance is a function of emissivity as well as surface temperature, multispectral imaging systems are needed to separate the effects of temperature and emissivity. Realmuto et al. [1992] demonstrated the separation of temperature and emissivity effects in the mapping of an active Hawaiian lava flow field. The launch of ASTER in 1998 [Kahle et al., 1991] will permit the collection of multispectral TIR image data on a global, rather than local, scale.

2.3 Instrument Characteristics

The principal data set for this algorithm will be acquired by ASTER. A brief description of the characteristics of this instrument is found in this section. A more detailed discussion of ASTER can be found in Kahle et al. [1991]. The specifications for the fourteen ASTER channels are listed Table 1.

As indicated by the table, the ASTER instrument is actually a collection of three separate imaging sub-systems, each operating in a separate spectral region. The visible and near-infrared (VNIR) subsystem features nadir and forward-looking telescopes to provide panchromatic stereographic coverage in ASTER Channel 3.

All three of the imaging subsystems will have crosstrack pointing capability of at least 8°. The crosstrack pointing, together with the 16-day repeat cycle of the EOS AM-1 platform, will enable ASTER to image virtually any point on Earth. Due to operational constraints, ASTER will probably acquire fewer than 50 volcano images per year.

3. ALGORITHM DESCRIPTION

3.1 Theoretical Description

The change detection procedure is based on Student's t test. This test determines the likelihood that the mean of a limited set of samples is an accurate measure of the mean of the population from which the samples are drawn. The test is also used to determine the likelihood that two sets of samples come from the same population.

The Student's t statistic is calculated using the mean and standard deviation of the sample set:

$$t = \frac{\sqrt{N}(X - \mu_0)}{s}$$

where N is the number of observations in the sample set, X is mean of the sample set, μ_0 is the hypothetical mean of the population, and s is the standard deviation of the sample set.

The shape of Student's probability distribution, $P(t)$, is a function of N , which is also known as the number of degrees of freedom. Student's distribution is symmetric about $t = 0$, which represents the hypothesis that the sample mean (X) is equal to the population mean (μ_0). The variance of $P(t)$ is $(N - 1)/(N - 3)$, which approaches 1 when N is large. For $N > 4$, $P(t)$ resembles a Gaussian probability distribution with a mean of zero and unit variance.

The larger the difference between X and μ_0 , the smaller the probability of the test statistic. This probability is known as the confidence or significance level of the Student's t test. For example, if the probability of t is 0.05, then the difference between X and μ_0 is significant at the 5% level. Alternatively, we can be 95% confident that X is different than μ_0 . We perform a Student's t test by first selecting N and a level of confidence and determining the value at which $1 - P(t_0)$ is equal to the confidence level. If our test statistic t is larger than t_0 , we can reject the hypothesis that $X = \mu_0$.

As noted above, $P(t)$ becomes more narrow (variance approaches unity) as N increases. Since an increase in N also produces an increase in the test statistic, it becomes easier to reject the hypothesis that $X = \mu_0$ as the number of samples increases. However, an increase in N can result in an increase in the sample standard deviation (s) if the data are noisy. An increase in s can reduce the size of the test statistic, making it more difficult to reject the hypothesis.

The application of Student's t test to the detection of temporal changes in surface temperature is straightforward. Temporal changes in temperature can result from seasonal variations in local weather conditions or diurnal changes in solar heating. Our goal is to separate geothermally-induced temperature changes from those due to diurnal or seasonal effects. We seek the localized changes in temperature (X), which we assume to be related to geothermal activity, that are significantly different than the regional changes in temperature (μ_0), which we assume to be related to diurnal or seasonal effects. The significance of a geothermal anomaly is a function of its area (relative to N) and the level of noise in the data (s).

For application to image data, the Student's t test is implemented as a moving window algorithm. The value of the t statistic at each window location is a function of the window size together with the mean and standard deviation of the pixels that fall within the moving window.

The criterion for rejecting the hypothesis is a function of the window size and confidence level, which do not change with window location.

3.2 Practical Considerations

The current version of the change detection procedure was developed on a Sun 4/80 (SPARCstation 10) with 160 Mbytes of physical memory (RAM) and 435 Mbytes of virtual memory. XCHANGE2 will run on computers with less than 160 Mbytes of RAM, but it is important to note that the memory requirements of the procedure can be large. The mean, standard deviation, and Student test statistic are calculated using IDL array operations, which require that all the necessary floating point array buffers be held in memory during operation of the procedure. The output change map is held in memory as a byte array until the map is saved to a disk file.

3.2.1 Operation of Procedure

An IDL-based application known as XCHANGE2 has been developed to perform the change detection procedure described in this document. IDL provides a graphic user interface which allows the input data sets, and the window size, confidence level, and population mean used in the Student's t test to be modified interactively. A copy of the on-line help document for XCHANGE2 and examples of data products created with this application can be found in the Appendices.

The initial inputs to XCHANGE2 are two image data sets. These images must be in spatial registration with one another. IDL array operations are used to subtract one input image from another and calculate the local mean, standard deviation, and test statistic for each pixel location in the resulting difference image. The rejection criteria are calculated from the number of degrees of freedom (N), which is defined by the size of the moving window, and the desired level of confidence. The IDL statistics package contains routines for the calculation and analysis of Student's probability distribution, $P(t)$.

On default, XCHANGE2 uses a window size of 3 X 3 ($N = 8$) and confidence level of 0.95. The mean of the entire difference image is calculated for use as the population mean (μ_0). As noted above, any of these parameters can be modified through the graphic user interface. XCHANGE2 can be used to build up thematic maps, where each theme represents a different combination of window size, confidence level, and population mean. The digital number (DN) used to represent an individual theme in the change map is specified by the user. The default DN is 255.

3.2.2 Input Data Requirements

The primary input data set for the change detection algorithm will be ASTER registered radiance at the sensor (AST03, parameter # 2452). The size of AST03 is 243 Mbytes per 60 X 60 km ASTER scene, and two scenes will be required for each change map.

The preparation of a change map from AST03 requires that (1) the radiance data be corrected for atmospheric effects, and (2) we recover a estimate of surface temperature from the ASTER radiance measurements. Prior to the launch of the EOS PM-1 platform in 2001, the primary source of profiles of atmospheric temperature and water vapor will be MODIS atmospheric temperature (MOD30, parameter # 3726) and moisture (MOD30, parameter # 3727) profiles. These products will be available at a spatial resolution of 5 km X 5 km, and 12 MODIS temperature and humidity profiles will be used to cover an 60 km X 60 km ASTER scene. The MOD30 profiles are combined into a data record containing 237 bytes, so approximately 3 kbytes of MODIS product will be required per ASTER scene.

Following the launch of the EOS PM-1 platform in 2001, data collected with the Atmospheric Infrared Sounder (AIRS)/Advanced Microwave Sounding Unit (AMSU) experiment will be incorporated into the change mapping procedure. These relevant AIRS data products are the atmospheric temperature (AIR07, parameter # 1588) and humidity profiles (AIR05, parameter # 1828). The size of the AIRS data products has yet to be determined, but the profile data should be on the order of 1500 bytes. In addition to MODIS and AIRS/AMSU data products, atmospheric profile data will be obtained from a variety of ancillary sources, such as radiosoundings, climatology models, and assimilation models.

We note here that ASTER will offer a surface (kinetic) temperature product, AST08 (parameter # 3803). AST08 will be generated from AST09 (parameter # 3817), surface radiance, and AST09 will be derived using the methods and data sets described above. In addition, AST08 will be corrected for variations in spectral emissivity. Given the Volcanology Team's objective of producing at least 11 change maps per year, we will seriously consider the use of AST08 as a time-savings measure.

The substitution of AST08 for AST03 would decrease our input data volume from 500 Mb/scene (which includes the MODIS and AIRS profile data) to 4 Mb/scene. One drawback to this substitution is that AST08 will be calculated from the ASTER TIR channels. High-temperature surfaces radiant in the SWIR or VNIR may therefore be misrepresented in this data product.

3.2.3 Output Data Products

Our experiment plan is to produce bi-monthly temperature change maps for three select volcanoes with a contingency of four extra maps to document unexpected eruptions. The total production will be at least 11 maps per year.

The size of the output products will be approximately 1.3 Mb/map if the change maps are produced in a 24-bit raster format. Producing the final maps in an 8-bit color graphics format such as GIF or HDF will reduce the data volume to approximately 0.5 Mb/map. Our total output data volume will be at least 14 Mb/year (5.5 Mb/year for GIF or HDF).

4. CONSTRAINTS, LIMITATIONS, AND ASSUMPTIONS

The descriptions of the mathematics involved in creating the change-detection maps are deceptively simple, since the most intense number crunching accomplished by the array operations of IDL. We assume that the Land Processes Distributed Active Archive Center (LP- DAAC) at the USGS EROS Data Center (EDC) will accept procedures written in IDL and that any users requesting copies of the procedure will have their own copies of IDL. We further assume that there will be no violation of copyright or distribution agreements if the EDC or any member of the Volcanology IDS team distributes software written in IDL.

The registration of image data products can be a formidable task. We are assuming that the inherent geometric fidelity of data acquired from satellite platforms (relative to data acquired from an aircraft) will minimize the effort required to do the registration. However, ASTER is designed to point off nadir, and these data products may prove to be much more difficult to register.

5. REFERENCES

- Abrams MJ, Buongiorno M-F, Realmuto VJ, Pieri DC (1994) Mount Etna lava flows analyzed with remote sensing. *EOS Trans AGU* 75: 545
- Bianchi R, Casachia R, Coradioni A, Duncan AM, Guest JE, Kahle AB, Lanciano P, Pieri DC, Poscolieri M (1990) Remote sensing of Italian volcanoes. *Trans Am Geophys Union* 71: 1789-1791
- Bonneville A, Gouze P (1992) Thermal survey of Mount Etna volcano from space. *Geophys Res Lett*: 725-728
- Davis JC (1973) *Statistics and Data Analysis in Geology*. Wiley, New York, New York, pp 1- 550
- Dzurisin D, Denlinger RP, Rosenbaum JG (1990) Cooling rate and thermal structure determined from progressive magnetization of the dacite dome at Mount St. Helens, Washington. *J Geophys Res* 95: 2763-2780
- Fischer WA, Moxham RM, Polcyn F, Landis GH (1964) Infrared surveys of Hawaiian volcanoes. *Science* 146: 733-742
- Flynn LP, Mougini-Mark PJ, Horton KA (1994) Distribution of thermal areas on an active lava flow field: Landsat observations of Kilauea, Hawaii, July 1991. *Bull Volcanol* 56: 284-296
- Frieden BR (1983) *Probability, Statistical Optics, and Data Testing*. Springer-Verlag, New York, pp 1-404
- Friedman JD, Williams RS (1968) Infrared sensing of active geologic processes. *Proc Fifth Symp Remote Sens Environ*: 787-820
- Friedman JD, Williams RS (1970) Changing patterns of thermal emission from Surtsey, Iceland between 1966 and 1969. *US Geol Surv Prof Paper* 700-D: D116-D124
- Friedman JD, Frank D (1980) Infrared surveys, radiant flux, and total heat discharge at Mount Baker volcano, Washington, between 1970 and 1975. *US Geol Survey Prof Paper* 1022-D
- Friedman JD, Frank D, Kieffer HH, Sawatzky DL (1981) Thermal infrared surveys of the May 18 crater, subsequent lava domes, and associated volcanic deposits. *US Geol Survey Prof Paper* 1250: 279-294
- Friedman JD, Williams DL, Frank D (1982) Structural and heat flow implications of infrared anomalies at Mt. Hood, Oregon, 1972-1977. *J Geophys Res* 87: 2793-2803
- Gaonac'h H, Vandemeulebrouck J, Stix J, Halbwachs M (1994) Thermal infrared satellite measurements of volcanic activity at Stromboli and Vulcano. *J Geophys Res* 99: 9477- 9486
- Kahle AB, Palluconi FD, Hook SJ, Realmuto VJ, Bothwell G (1991) The Advanced Spaceborne Thermal Emission and Reflectance Radiometer (ASTER). *Int J Imaging Sys Tech* 3: 144-156
- Kieffer HH, Frank D, Friedman JD (1981) Thermal infrared surveys of Mount St. Helens - observations prior to the eruption of May 18. *US Geol Survey Prof Paper* 1250: 257-278
- Mastin LG (1994) Explosive tephra emissions at Mount St. Helens, 1989-1991: the violent escape of magmatic gas following storms? *Geol Soc Am Bull* 106: 175-185
- Mougini-Mark PJ, Garbeil H, Flament P (1994) Effects of viewing geometry on AVHRR observations of volcanic thermal anomalies. *Remote Sens Environ* 48: 51-60
- Moxham RM (1970) Thermal features of volcanoes in the Cascade Range as observed by aerial infrared surveys. *Bull Volcanol* 34: 77-106
- Palmason G, Friedman JD, Williams RS, Jonsson J, Seamundsson K (1970) Aerial infrared surveys of Reykjanes and Torfajokull thermal areas, Iceland, with a section on cost of exploration surveys. *Geothermics* 2: 399-412
- Realmuto VJ, Hon K, Kahle AB, Abbott EA, Pieri DC (1992) Multispectral thermal infrared mapping of the 1 October 1988 Kupaianaha flow field, Kilauea volcano, Hawaii. *Bull Volcanol* 55: 33-44

Table 1: Characteristics of the ASTER Channels

| Specifications for ASTER Channels | | | |
|-----------------------------------|-------------|-------------------------------|---------------------------|
| Subsystem | Band Number | Bandpass (μm) | Spatial Resolution (m) |
| VNIR | 1 | 0.52 - 0.60 | 15 |
| VNIR | 2 | 0.63 - 0.69 | 15 |
| VNIR | 3 | 0.76 - 0.86 | 15 |
| SWIR | 4 | 1.600 - 1.700 | 30 |
| SWIR | 5 | 2.145 - 2.185 | 30 |
| SWIR | 6 | 2.185 - 2.225 | 30 |
| SWIR | 7 | 2.235 - 2.285 | 30 |
| SWIR | 8 | 2.295 - 2.365 | 30 |
| SWIR | 9 | 2.360 - 2.430 | 30 |
| TIR | 10 | 8.125 - 8.475 | 90 |
| TIR | 11 | 8.475 - 8.825 | 90 |
| TIR | 12 | 8.925 - 9.275 | 90 |
| TIR | 13 | 10.25 - 10.95 | 90 |
| TIR | 14 | 10.95 - 11.65 | 90 |

APPENDICES

APPENDIX A: Examples of Output from XCHANGE2

Figure A.1 depicts a pair of temperature maps for the lava dome of Mount St. Helens Volcano. These maps were produced from TIMS data acquired on 22 September 1989 and 30 March 1991. Both data sets were acquired before dawn to eliminate the effects of solar heating.

Each data set was registered to a 1:4000 scale digital elevation model (DEM) of the Mount St. Helens crater and dome, thus bringing the two data sets into registration with one another. The resolution of the DEM was 3 m in both the horizontal and vertical dimensions. The spatial resolution of the registered TIMS data is therefore a factor of 30 better than that planned for the ASTER thermal channels.

Overall, the surface temperature of the dome and crater was much lower in March 1991 than in September 1989 (Fig. A.1). In the month prior to the 1991 overflight 16 cm of precipitation had fallen on Mount St. Helens, and snow blanketed the lava dome. In contrast, only 4 cm of precipitation fell in the month prior to the 1989 overflight. Despite the presence of snow, the temperatures of the hottest points measured in 1991 are comparable to those measured at the same points in 1989. The maintenance of hot spot temperatures at the surface of the dome in 1991 was probably due to the efficient transport of heat from the interior of the dome via the circulation of meltwater [cf. Dzurisin et al., 1990].

The appearance of two new hot spots in the 1991 temperature map (Fig. A.1) mark the sites of the North (designated as A) and East (designated as B) vents [Mastin, 1994]. The North vent was the site of five explosive emissions of tephra between 7 December 1989 and 14 February 1991. The East vent was the site of explosions on 20 December 1990 and 5 February 1991. Tephra was emitted from both vents during the 5 February 1991 event. Mastin [1994] demonstrated the correlation between the explosive events and increases in precipitation.

The application of the change-detection algorithm to the Mount St. Helens data of Figure A.1 is presented in Figure A.2. Figure A.2a is a color-contour map of the differences between the 1991 and 1989 temperature map. The contour map shows the locations where the temperature was higher in 1991 than in 1989. There were many locations where the 1991 temperatures were higher, with the largest positive temperature changes clustered on the northern and southeastern sectors of the dome.

Due to the intervening activity, ground temperatures at the North and East vents (cf. Fig. A.1) were > 25 °C hotter in 1991. Positive differences in excess of 25 °C were also present on the northeast sector of the dome, between the North and East vents, and locations on the southeast sector. Most of the positive differences on the southeastern sector were between 15 and 25 °C.

Figures A.2b - d contain thematic change maps produced with XCHANGE2. Figure A.2b depicts the effects of changing the confidence level used in Student's t test while holding the window size at 3 X 3 (N=8). The population mean (μ_0) was set at 0 °C to map the locations where the 1991 dome was significantly hotter than the 1989 dome. Figure A.2b indicates that the confidence level used to map the changes had little influence on the change map. The level of confidence for the majority of the positive changes is greater than 0.95. The strong temperature contrast between the hot spots and the snow blanket of 1991 contributes to the lack of ambiguity over the positive temperature changes.

Figure A.2c shows the effect of changes the size of the moving window, which changes the number of degrees of freedom (N). The confidence level was set to 0.95 and the population mean (μ_0) was set to 0°C. The North and East vents (cf. Fig. A.1) are clearly identified in this thematic map, as are the hot spots in the northeastern and southeastern sectors of the dome. Figure A.2c indicates that an increase in window size, which increases N, is a good technique for identifying the most intense changes in temperature. In general, an increase in the window size (N) results in an increase in the local standard deviation (s) with relatively little change in the local mean (X). This general behavior causes a decrease in Student's t statistic, which makes the hypothesis that $X = \mu_0$ more difficult to reject. In the presence of a hot spot, an increase in window size results in a

decrease in μ_0 with relatively less change in s . For areas where the temperature difference is large, this decrease in μ_0 has less impact on Student's test statistic and the hypothesis is rejected.

Figure A.2d shows the effects of changing the hypothesis while holding the window size at 3×3 ($N=8$) and the confidence level at 0.95. This thematic map shows that the temperature differences at North vent, East vent, and the hot spots on the northeastern and southeastern sectors of the dome are significantly greater than 10°C .

The test results presented in Figure A.2 suggest that a simple contour map of positive temperature changes on the dome (Fig. A.2a) is as informative as any of the thematic maps produced with XCHANGE2, which are more complicated data products. This result is due to the strong contrast between hot spots on the 1991 dome and the cold snow blanket. In a more general application the hot spots are apt to be less distinct against the background, due to higher ambient ground temperatures, noise in the data, or coarse spatial resolution, and the spatial context of the change-detection procedure will be more beneficial. In any event, the change-detection procedure allows us to state the confidence with which the temperature changes are mapped.

Figure A.1

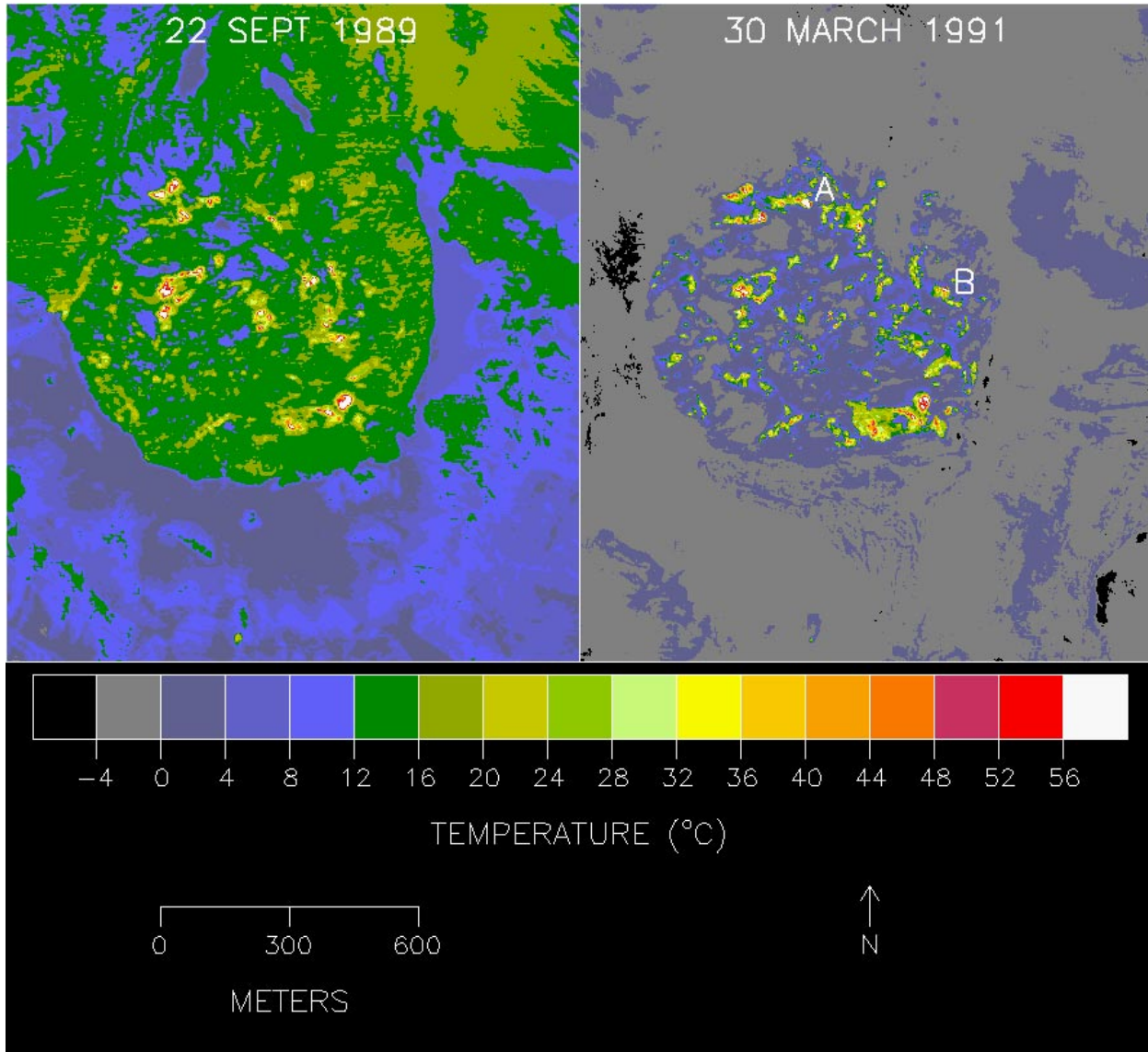
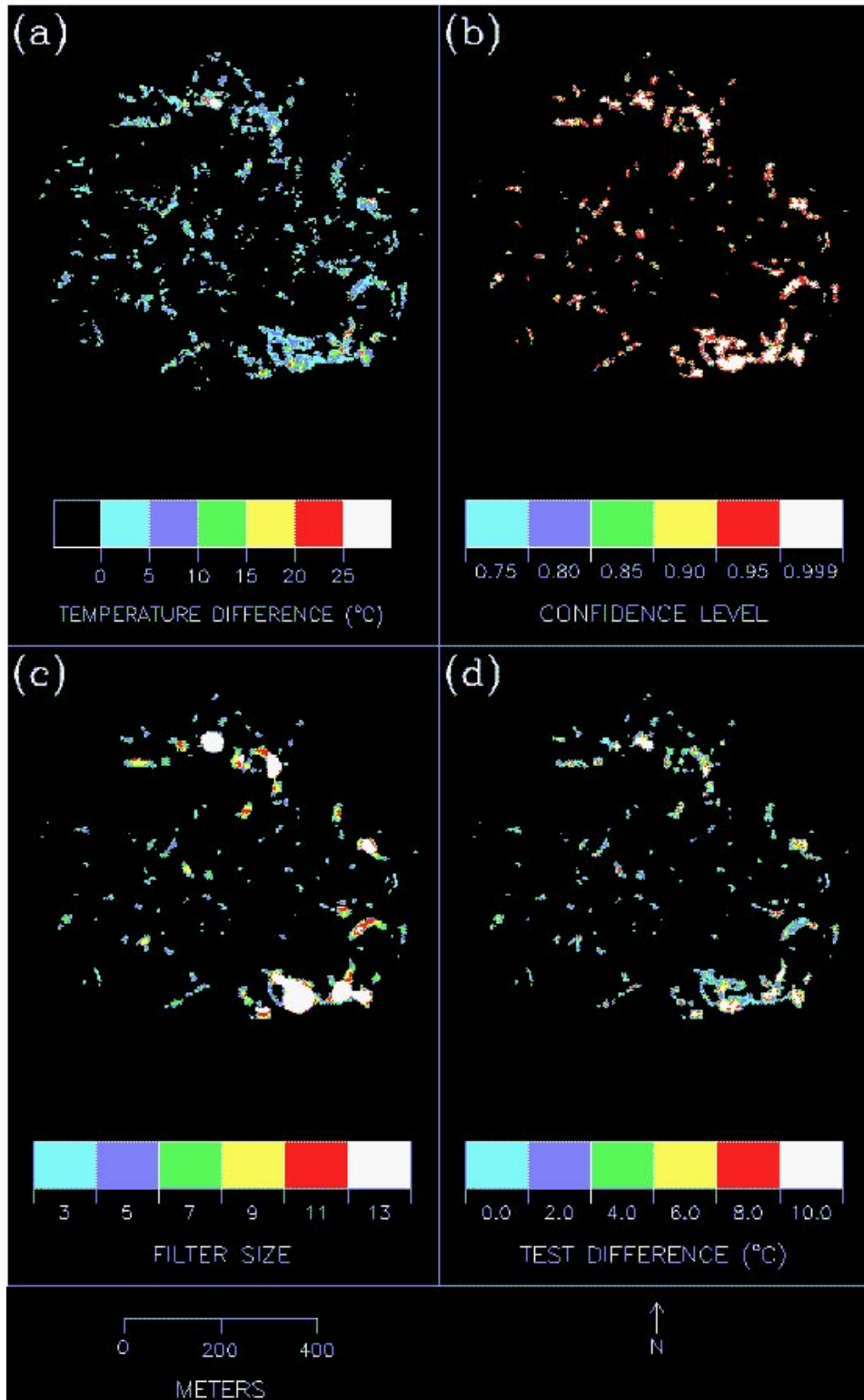


Figure A.2



APPENDIX B. XCHANGE2 On-line Help Documentation

INTRODUCTION

XCHANGE2 is a graphic user interface to a change detection algorithm based on Student's t Test. A review of this test can be found in most introductory textbook on statistical testing. Student's t Test allows us to test the hypothesis that the mean of a limited number of samples is equal to the mean of the population from which the samples were drawn. The test factors in both the number of samples and level of noise (variation) in the sample set.

XCHANGE2 is intended to be used to detect temporal changes in the surface temperatures of volcanic and geothermal features. Student's t Test is used to separate localized changes in temperature, which we assume to be related to changes in geothermal activity, from regional changes in temperature, which are related to diurnal or seasonal effects. We seek local changes in temperature (sample means) that are significantly different from the regional change (population mean).

The criterion for rejecting the hypothesis that the local changes in temperature are equal to the regional change in temperature is a function of the number of local samples and the desired confidence in the rejection. Both of these parameters may be specified by the user.

The graphic user interface to XCHANGE2 consists of two widgets. The first is a dialog widget, which is used to enter user-specified parameters. the second is a display widget, which is used to display the difference image, change map, and a variety of local parameters.

OPERATION OF XCHANGE2

Upon initiation of XCHANGE2, the dialog widget pops up on the screen. You must specify the file names of the two images that are to be compared. In most instances, these inputs will be a pair of temperature maps each depicting the surface temperatures of a volcanic or geothermal region at different points in time. The maps must be coregistered, and the temperatures must be stored in the same data units. The file names are entered by clicking on the respective input buttons (INPUT IMAGE #1 and #2) and choosing the names from a pop-up list widget. In this version of XCHANGE2, the input images must be in the JPL VICAR format. XCHANGE2 get the size of the image and data format from VICAR labels, which are typically the first record of an image file. Future versions of XCHANGE2 will accept input images without VICAR labels.

Once the file names are specified, a click on the BEGIN button causes the display widget to appear on the screen. The left display port shows the difference image created by subtracting input image #2 from image #1. The input images are converted to floating point values prior to this subtraction. The right display port will display the change map, which is built-up sequentially in the process described below. The clicking the left mouse button while the cursor is inside either display port will cause the line and sample position of that point to be reported in the bottom panel of the display widget. A collection of local values, which are described below, are also reported in this panel.

XCHANGE2 is based on a moving-window procedure, much like a spatial filtering algorithm. You specify the size of this window in the dialog widget. The default window size of 3 X 3 is also the smallest size that is accepted by XCHANGE2. The window is scanned through the difference image and Student's t statistic (LOCAL T STAT) is calculated at each window position. The test statistic is a function of the local mean (LOCAL MEAN), standard deviation (LOCAL STDV), which change with the position of the window.

The rejection criterion (REJ CRIT), which is based on the window size and the desired confidence

in the rejection, does not change with window position. You can specify the desired confidence level (CONFIDENCE LEVEL) in the dialog widget.

In default mode, XCHANGE2 uses the scene mean (SCENE MEAN in the display widget) to calculate the local test statistics. In this mode, the local means are tested against the scene mean. However, you may wish to test the local changes in temperature against a different value. For example, you may wish to identify all pixels at which the local change in temperature is greater than zero. To perform this test, enter zero as the POPULATION MEAN in the dialog widget. To test any hypothesis, click on MAP CHANGES in the dialog widget.

The pixel locations at which the hypothesis was rejected are marked with the CHANGE MAP VALUE, and the change map is loaded into the left view port of the display widget. You can specify any map value between 0 and 255. The CLEAR MAP button erases the change map, while the PSEUDO COLOR button pops up a list widget that allows you to view the change map as a color-contour map.

The SAVE button allows you to save the change map to a disk file. Note that the saved change map will not be a 24- or 8-bit (ie: GIF, TIFF, or HDF) image, even if you used PSEUDO COLOR to view a color-contour map. Currently, the saved change map is in byte format, with a VICAR label as the first record. Future versions of XCHANGE2 will let you choose the format of the output map.

Happy Mapping!!!